Coordination Chemistry Reviews 253 (2009) 2315–2327

Contents lists available at ScienceDirect

Coordination Chemistry Reviews

journal homepage: www.elsevier.com/locate/ccr

Review

Polyoxometalates: Fascinating structures, unique magnetic properties

Ulrich Kortz[a,*], Achim Müller[b], Joris van Slageren[c,d], Jürgen Schnack[e], Naresh S. Dalal[f], Martin Dressel[c]

[a] School of Engineering and Science, Jacobs University, P.O. Box 750561, 28725 Bremen, Germany
[b] Fakultät für Chemie, Universität Bielefeld, Postfach 100131, 33501 Bielefeld, Germany
[c] 1. Physikalisches Institut, Universität Stuttgart, Pfaffenwaldring 57, D-70550 Stuttgart, Germany
[d] School of Chemistry, University of Nottingham, Nottingham NG7 2RD, UK
[e] Fakultät für Physik, Universität Bielefeld, Postfach 100131, 33501 Bielefeld, Germany
[f] Department of Chemistry and Biochemistry, Florida State University and National High Magnetic Field Laboratory, Tallahassee, Florida 32306-4390, USA

Contents

ARTICLE INFO

Article history:
Received 17 October 2008
Accepted 15 January 2009
Available online 23 January 2009

In memoriam Dr. Karlheinz Schmidt.

Keywords:
Polyoxometalates
Transition metals
Lanthanides
Magnetism
Electron spin resonance

ABSTRACT

We report on several discrete molecular transition metal- and lanthanide-containing polyoxo-tungstates and -molybdates with a focus on their magnetic properties. The polyanions discussed here all contain 3d paramagnetic centers and are mostly of the spherical $\{Mo_{132}\}$ Keplerate type, the cyclic $\{P_8W_{48}\}$ type, the dimeric $\{X^{III}_2W_{18}\}$ (X = As, Sb) type, and the dimeric, fused $\{Si_2W_{18}\}$ type. The number of incorporated magnetic ions in the structures described here ranges from 3 to 30.

1. Introduction

In a review about polyoxometalates (POMs) which shows an unusually high citation of ca. 1500, indicating highly enthusiastic acceptance of our chemistry worldwide, we can read [1a]: "*Polyoxometalates form a class of inorganic compounds that is unmatched in terms of molecular and electronic structural versatility, reactivity, and relevance to analytical chemistry, catalysis, biology, medicine, geochemistry, materials science, and topology*." This statement has remained undisputed since its publication in 1991. The polyoxomolybdates (under reducing conditions) are in general considered unique [1b] as far as the variety of molecular

* Corresponding author.
E-mail address: u.kortz@jacobs-university.de (U. Kortz).

0010-8545/$ – see front matter © 2009 Elsevier B.V. All rights reserved.
doi:10.1016/j.ccr.2009.01.014

structures is concerned. Their importance for aspects of molecular magnetism – this also in context with materials science – can be directly recognized by reading the latest monograph in this field entitled "*Molecular Nanomagnets*" [1c] where 10 pages are devoted to this topic (for general related reviews see also Ref. [1d–f]). In this context, it was argued in the title of a subsequent review that POMs represent a "*Source of Unusual Spin Topologies*" [1g]. Books related to POM chemistry, also including their magnetic properties, are listed under [1h–l]. Some POMs show slow relaxation of the magnetization and function as single-molecule magnets [2].

Much attention has been focused on the $\{V^{IV}{}_{15}\}$ type cluster, which was synthesized 20 years ago [3], leading to about 60 papers concerning its remarkably versatile magnetic properties which have been published in the meantime (see, e.g. Ref. [4] and Section 14.3.2 of Ref. [1c]). It exhibits layers of different magnetization including a V^{IV} triangle responsible for frustration effects. Important for several of the properties is the low $S = 1/2$ spin ground state in a comparably large cluster. Furthermore, these clusters allowed – embedded in surfactants – the first observation of Rabi oscillations in a molecular magnet [4f].

Of enormous interest are those clusters where the electronic charges are not originally localized on individual ions, but can hop from one side to the other (therefore considered as models for magnetic conductors!). Charge delocalization in Robin and Day types II and III mixed valence clusters [5] can cause strong increase of the spin coupling [6]. In this context the $\{V_{18}O_{42}\}$ type clusters were described as the most versatile ones (Section 14.3.3 of Ref. [1c]) especially as two forms exist with T_d and D_{4d} symmetry and the electron populations can be varied over a wide range, i.e. between 10 and 18 3d-V electrons [7]. A detailed study of the $\{V^{IV}{}_6V^{V}{}_6\}$ type cluster was performed regarding the interesting intramolecular charge transfer [8]. One manifestation of charge delocalization is the double exchange mechanism, which leads to strong ferromagnetic spin coupling [9].

Clusters of the type $\{M_6Mo_{57}\}$ ($M = V^{IV}$, Fe^{III}, Cu^{II}) were also considered to be of general interest as M can be successively substituted and in the case of $M = V^{IV}$ extremely strong exchange coupling is observed due to strong electron delocalization, a scenario which is completely different for $M = Fe^{III}$ [10]. The magnetization of the system becomes anisotropic at low field.

Polyoxotungstates are ideal candidates for the incorporation of multinuclear magnetic transition metal clusters [1h–l]. This is largely due to the existence of a large number of vacant, stable polytungstate precursors (as opposed to polymolybdates or polyvanadates). The number of vacant sites in a single lacunary polytungstate can range from 1 (e.g. $[SiW_{11}O_{39}]^{8-}$) to 2 (e.g. $[\gamma\text{-}SiW_{10}O_{36}]^{8-}$), to 3 (e.g. $[P_2W_{15}O_{56}]^{12-}$), to 6 (e.g. $[H_2P_2W_{12}O_{48}]^{12-}$) all the way to 20 (e.g. $[H_8P_8W_{48}O_{184}]^{32-}$) [1k,l]. Formation of dimeric, trimeric, tetrameric, etc. assemblies can therefore allow for encapsulation of a large number of spin-coupled magnetic centers (d- or f-block), usually bridged via μ_2-oxo/hydroxo/aqua groups. This means that many different shapes, sizes and types of magnetic clusters can be stabilized by polytungstate ligands. Furthermore, the diamagnetic tungsten-oxo capping fragments isolate the respective magnetic clusters so well from each other that intermolecular interactions are usually negligible. This means that detailed and subtle magnetic phenomena can be studied strictly on the molecular level [1e].

Magnetic POMs have also provided convincing experimental evidence for the occurrence of anisotropic exchange interactions in exchange coupled clusters. Thus, inelastic neutron scattering studies on POMs containing a Co_3 cluster showed not only that anisotropic exchange interactions definitively occur in these systems, but also that the anisotropic exchange interaction tensors may be nonparallel [11]. Antisymmetric exchange interactions were also found in Cu_3 POMs [12], and in the previously mentioned $\{V_6Mo_{57}\}$ cluster [10]. Generally speaking, direct evidence for antisymmetric exchange in exchange coupled clusters is quite scarce [13]. Nickel(II) containing polytungstates were investigated in detail using inelastic neutron scattering in addition to magnetic measurements, which enabled the determination of single-ion anisotropies as well as isotropic exchange interaction parameters [14].

A particularly interesting and popular system is represented by the aesthetically beautiful spherical multifunctional clusters of the type $\{M_{30}Mo_{72}\}$ ($M = OV^{IV}$, Cr^{III}, Fe^{III}) called Keplerates (Ref. [15] and Section 14.3.1 of Ref. [1c]) containing the unique M_{30} icosidodecahedron with 60 equal edges, which apart from novel magnetic behaviour as polyprotic acids show a new type of assembly process in solution leading to unprecedented "magnetic" vesicles and inorganic membranes. These clusters for which the spin can be varied ($S = 1/2$, $3/2$ and $5/2$) are considered to be of tremendous importance for the understanding of magnetism in Kagomé lattices, which are of interest for materials science [16] (see title: "*Highly frustrated magnetic clusters: The kagomé on a sphere*" [15e]). Furthermore, the $\{Fe_{30}Mo_{72}\}$ type cluster shows an unprecedented classical magnetic behaviour and competing spin configurations [15a]. For the construction of these Keplerates pentagonal units are the key building blocks (see Section 4.4.1 of Ref. [1c]).

In the following we will discuss some especially interesting magnetic POM-based clusters (polymolybdates and polytungstates) which have been a strong focus of our studies over the past decade or so.

2. Keplerates of the type $\{M_{30}Mo_{72}\}$ ($M = Fe^{III}$, Cr^{III}, V^{IV}, Ln^{III})

Many aesthetically pleasing objects, ranging from fullerenes to viruses, consist of linked pentagonal units. A variety of highly symmetric POMs was generated by joining pentagonal $\{(Mo)Mo_5\}$ units present in a dynamic library with deliberately chosen linkers. (Several molybdate species present in the related solution can interconvert.) The composition of this dynamic library depends critically on the experimental conditions, and this behaviour is unique to molybdates and not found for tungstates until now [17]. At low pH, the pentagonal structural unit occurs in the $[Mo^{VI}{}_{36}O_{112}(H_2O)_{16}]^{8-}$ anion, which is the only abundant species under those conditions. The complexes are then formed by a split and link process after adding the linker precursor. By utilization of dinuclear molybdate linkers 12 pentagonal units are connected by 30 linkers forming diamagnetic $\{Mo_{132}\}$ clusters. The structure contains pores that are large enough to be permeable to small cations, and its charge can be tuned to a great extent by ligand substitution. Indeed, reaction of $\{Mo_{132}\}$ clusters with different cations led to trapping of these cations at well-defined positions within the capsules [18]. In this manner, a range of paramagnetic derivatives $\{M_nMo_{132}\}$ was generated containing transition metal or lanthanide cations, with $M = VO^{II}$, Mn^{II}, Fe^{III}, Co^{II}. Ni^{II}, and Pr^{III} in varying amounts (some unpublished). Because of long and inefficient pathways, the spins in these systems are essentially independent of each other and no indication of coupling between them was found [19].

2.1. $\{Fe_{30}Mo_{72}\}$

This cluster can be obtained in a facile synthesis (used worldwide by many groups) by the exchange of dinuclear $\{Mo_2{}^{V}O_4\}^{2+}$ linkers of $\{Mo_{132}\}$ with the mononuclear Fe^{III} linkers. The 30 iron(III) ions span an icosidodecahedron with virtual I_h symmetry, which is the origin of the extraordinary interest in the magnetic properties of $\{Fe_{30}Mo_{72}\}$ (see above). Oxidation of the binuclear linkers of $\{Mo_{132}\}$ leads to three $\{Mo_2{}^{VI}O_{8/9}\}^{n-}$ type units which act as internal ligands found on different underoccupied positions [20]. Recently, a new synthesis of this cluster was reported not

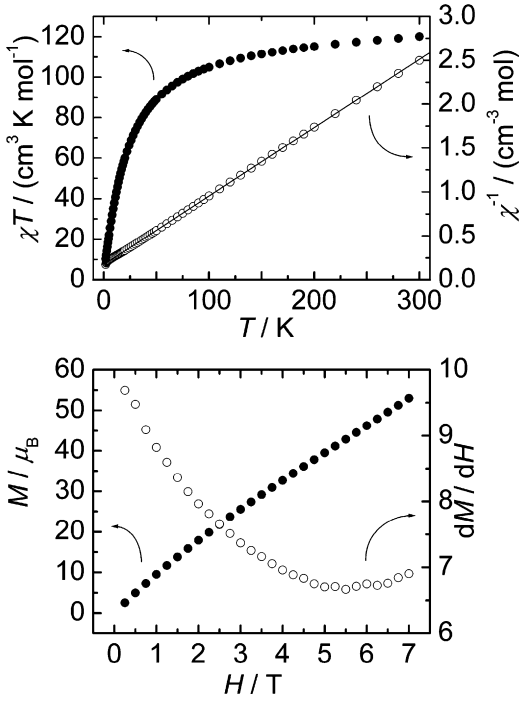

Fig. 1. $\{Mo_6\} \subset \{Fe_{30}Mo_{72}\}$ (upper panel) χT vs. T (filled circles, left axis) and χ^{-1} vs. T (open circles, right axis) measured at 0.1 T applied field. The solid line is a fit to the Curie–Weiss law $\chi^{-1} = (T - \theta)/C$. The lower panel shows the magnetization vs. field at $T = 1.8$ K (closed circles, left axis) and its numerical derivative (open circles, right axis). Taken from Ref. [21].

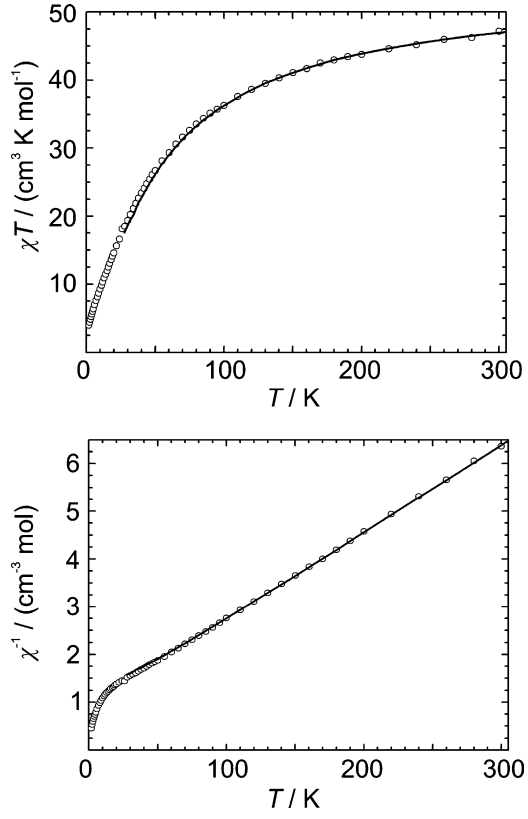

Fig. 2. Experimentally obtained χT (upper panel) and χ^{-1} (lower panel) vs. temperature (symbols) and quantum Monte Carlo result (continuous curve) for $\{Cr_{30}Mo_{72}\}$ with $J/k_B = -8.7$ K and $g = 1.96$. Taken from Ref. [22].

containing the binuclear $\{Mo_2\}$ ligands [21]. Interestingly, a non-covalently bound hexanuclear molybdate cluster $[Mo_6O_{19}]^{2-}$ is in this case encapsulated inside the $\{Fe_{30}Mo_{72}\}$. The magnetochemical investigation of the complex showed that the properties are very robust to changes in the synthetic procedure, i.e. to the dependence of the encapsulated dinuclear $\{Mo_2\}$ type ligands (Fig. 1). The decrease in the χT product on lowering the temperature confirms the presence of predominantly antiferromagnetic exchange interactions, in agreement with the negative Weiss temperature of $\theta = -22.3 \pm 0.3$ K found from a linear fit of χ^{-1} versus T. This is virtually the same as the Weiss temperature found for the product of the original synthesis ($\theta = -21.6 \pm 0.1$ K), demonstrating that the properties are virtually identical. This is supported by the characteristic minimum in dM/dH versus field at ca. 6 T (Fig. 1).

2.2. $\{Cr_{30}Mo_{72}\}$

A thorough experimental study of the spin level structure of $\{Fe_{30}Mo_{72}\}$ is hindered by the fact that the isotropic exchange interaction is rather weak ($J/k_B = 1.57$ K) [15a], which causes the lowest excitations to have very low energies [15c]. The analysis is further complicated because the effect of the single-ion zero-field splitting may not be negligible. In addition, the magnetic properties of $\{Fe_{30}Mo_{72}\}$ were largely described in a classical framework, which is justified by the relatively large single-ion spin of $s = 5/2$. Decreasing the single-ion spin the classical picture eventually becomes invalid, and consequently this transition from classical to quantum magnetism is of high scientific interest. For these reasons we have synthesized the chromium(III) derivative from $CrCl_3 \cdot 6H_2O$ using similar reaction conditions as in the new procedure for $\{Fe_{30}Mo_{72}\}$ [22]. The resulting $\{Cr_{30}Mo_{72}\}$ cluster crystallizes in the same space group as the iron(III) derivative. The exchange interaction between the chromium(III) ions is antiferromagnetic as evidenced by the decrease in χT with decreasing temperatures. A fit using quantum Monte Carlo (QMC) methods yielded an antiferromagnetic exchange coupling value of $J/k_B = -8.7 \pm 0.2$ K (Fig. 2). Note that also the weak upturn in χ^{-1} with decreasing T around 50 K is reproduced rather well by the calculations. In spite of the long superexchange pathway (Cr^{III}–O–Mo^{VI}–O–Cr^{III}), the interaction is moderately strong rendering this cluster excellently suitable for detailed studies of the spin level structure, e.g. by inelastic neutron spectroscopy, to investigate the validity of the rotational band model, which was proposed for the description of the magnetic properties of these clusters [23]. Furthermore, magnetization studies in very high fields should reveal whether a minimum in the differential susceptibility dM/dH can be observed at one-third of the magnetization saturation field ($H_{sat} \approx 60$ T) similar to the case of $\{Fe_{30}Mo_{72}\}$.

2.3. $\{V_{30}Mo_{72}\}$

The vanadyl derivative of the $\{M_{30}Mo_{72}\}$ clusters is of special interest because the vanadyl spin is $s = 1/2$. The exchange geometry therefore displays great similarity to that of the two-dimensional Kagomé lattice, which is of enormous interest especially from the theoretical side. Being slightly oblate, the $\{V_{30}Mo_{72}\}$ cluster is not as symmetric as the iron and chromium derivatives [24]. In spite of the lower symmetry, the susceptibility can be very well fitted by quantum Monte Carlo calculations employing a single exchange coupling constant of $J/k_B = 245$ K (Fig. 3). The enormous value of J compared to those of the two other $\{M_{30}Mo_{72}\}$ clusters is due to the fact that the relevant vanadyl energy levels are in close proximity to those of the pentagonal units; this leads to an efficient spin coupling by electron delocalization (see above). For an $S = 1/2$ icosidodecahedron, the lowest spin excitation was calculated to be at $0.05J$, while the lowest energy transition within the lowest rotational band lies at $0.22J$ [25]. For the J value obtained, the excitation energies are

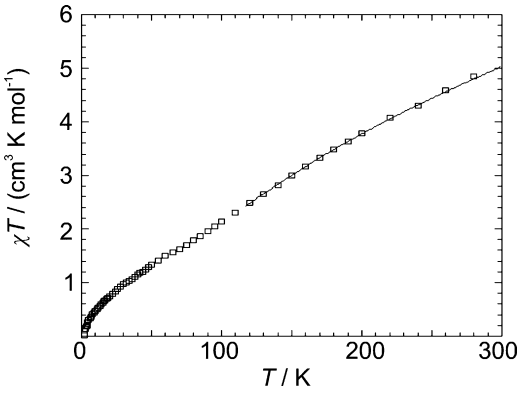

Fig. 3. Magnetic susceptibility χT of $\{V_{30}Mo_{72}\}$ vs. temperature: the experimental data are corrected for the two d^1/VO^{II} centers present in the crystal lattice (open squares); quantum Monte Carlo results fit the high-temperature data perfectly (solid curve). Taken from Ref. [24].

thus expected at 12 and 54 K, respectively. INS measurements on a nondeuterated sample showed a broad band between 4 and 11 meV, corresponding to 46 and 128 K [26]. However, the intensity of this band increases both with temperature and with momentum transfer, indicating that the band is due to phonon excitations. Polarized neutron scattering experiments on deuterated samples might be employed to detect eventually the presence of magnetic excitations under the phonon band.

2.4. $\{Ln_6Fe_{24}Mo_{72}\}$ (Ln = Ce, Pr)

Adding an aqueous solution of $LnCl_3 \cdot nH_2O$ to a solution of $\{Fe_{30}Mo_{72}\}$ results in the substitution of exactly six iron ions by lanthanide ions, which are disordered over 12 positions [27]. The capsules contain about two encapsulated lanthanide ions. The magnetic data are qualitatively similar to those of the parent compound $\{Fe_{30}Mo_{72}\}$ (Fig. 4). Hence it is not surprising that if the ions were uncoupled, the expected contributions of the cerium(III) and praseodymium(III) ions to χT would be a mere 6 and 11%, respectively. Even the Weiss temperatures are very similar to that of the parent complex, at $\theta = -27$ and -24 K, respectively. The main difference between the substituted complexes and the parent complex is the absence of the characteristic minimum in the differential susceptibility dM/dH at a field of 6 T for the former clusters. Apparently, the partial substitution has disturbed the symmetry to the extent that the picture of competing spin configurations is no longer valid.

3. The $\{Ni_4Mo_{12}\}$ Keggin-ion derivative

$[Mo_{12}O_{30}(\mu\text{-}OH)_{10}H_2\{Ni(H_2O)_3\}_4]$, henceforth abbreviated as $\{Ni_4Mo_{12}\}$, is a magnetic molecule comprised of Ni^{II} centers, which are positioned at the nucleophilic sites of an ε-Keggin cluster and thereby form an almost ideal tetrahedron [28]. Several of the other Ni clusters that are known [14,29] – among them also tetrahedral arrangements – exhibit ferromagnetic coupling between the Ni centers, and thus possess qualitatively different properties. In $\{Ni_4Mo_{12}\}$ the Ni^{II} ions are coupled antiferromagnetically along the rather long superexchange pathway (Ni^{II}–O–Mo^{VI}–O–Ni^{II}), which suggests a moderate coupling strength. Assuming perfect tetrahedral symmetry, the Heisenberg–Hamiltonian can be simplified by completing the square to

$$\hat{H} = -2J\sum_{k<l}\hat{s}_k \cdot \hat{s}_l = -J(\hat{S}^2 - 4s(s+1)) \quad (1)$$

where $\hat{s}_k$ are the Ni spin vector operators with spin quantum number $s = 1$ and $\hat{S}$ is the total spin operator with quantum numbers

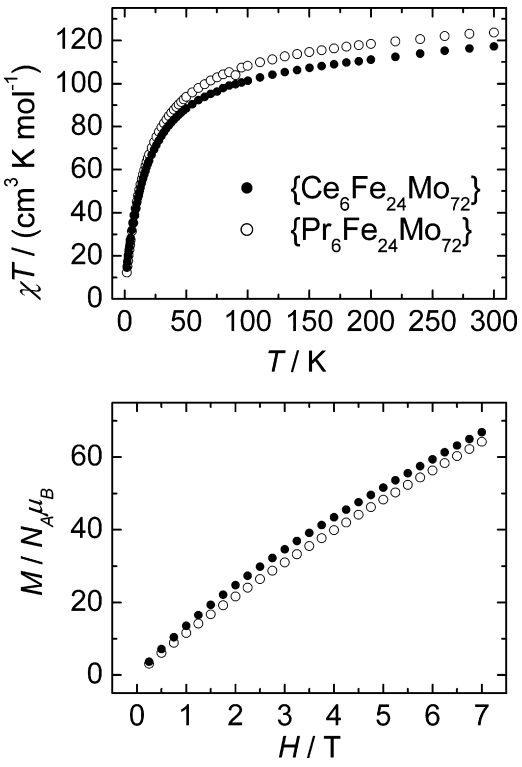

Fig. 4. χT as a function of temperature (upper panel) for $\{Ce_6Fe_{24}Mo_{72}\}$ (●) and $\{Pr_6Fe_{24}Mo_{72}\}$ (○) and the magnetization as a function of the field (lower panel) measured on powder samples. Taken from Ref. [27].

ranging from 0 to 4. The energy eigenvalues depend quadratically on the total spin thus forming a perfect rotational band. In an applied magnetic field, the lowest levels of adjacent multiplets therefore cross at equidistant field values. In a magnetization measurement at low temperatures the $M(H)$ curve should thus consist of four equal steps up to saturation. Fig. 5 demonstrates that this expectation is not met at all; on the contrary two smaller magnetization steps are followed by two steps with about twice the spacing [30]. The solid curve in Fig. 5 corresponds to the theoretical magnetization curve assuming a simple Heisenberg Hamiltonian with $J/k_B = -3.4$ K and an isotropic spectroscopic splitting factor $g = 2.25$. Although such a Hamiltonian reproduces the low-field susceptibility at $H = 0.5$ T rather well [30], it fails to describe the magnetization.

A thorough inspection of the available magnetization as well as EPR data leads to the conclusion that a minimal model for $\{Ni_4Mo_{12}\}$ should include additional terms. The following Hamiltonian was suggested:

$$\hat{H} = -\sum_{k,l} J_{kl}\hat{s}_k \cdot \hat{s}_l - \sum_{k,l,m,n} J^{biq}_{klmn}(\hat{s}_k \cdot \hat{s}_l)(\hat{s}_m \cdot \hat{s}_n) + \sum_k D_k(\vec{e}_k \cdot \hat{s}_k)^2 + \mu_B \sum_k \vec{B} \cdot g_k \cdot \hat{s}_k \quad (2)$$

The first term accounts for the superexchange coupling, where the matrix notation J_{kl} allows different exchange constants along the edges of the tetrahedron. This reflects the slight distortion of the tetrahedral symmetry. The second term is a generalized biquadratic term. Biquadratic terms with $k = m$ and $l = n$ are often used for Ni compounds; spin–phonon interaction is assumed as their physical origin [31]. Actually the restriction to $k = m$ and $l = n$ is unjustified since magnetoelastic coupling gives the remaining parts of the sum comparable strength. Quite recently another source of such terms was discussed [32]. It was pointed out that in the derivation of the

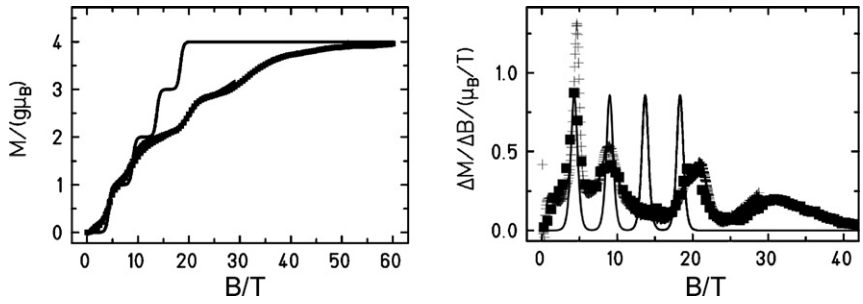

Fig. 5. (Left panel) Magnetization M as a function of applied magnetic field B: experimental data are given by squares (National High Magnetic Field Laboratory (NHMFL) at Los Alamos, $T = 0.44$ K; Okayama High Magnetic Field Laboratory (OHMFL), $T = 0.40$ K). The theoretical magnetization is given by a solid curve for $T = 0.44$ K. Here a simple Heisenberg Hamiltonian is assumed with $J/k_B = -3.4$ K and an isotropic spectroscopic splitting factor $g = 2.25$. In the right panel, the same data are shown as differential magnetization dM/dB. Taken from Ref. [33a,b].

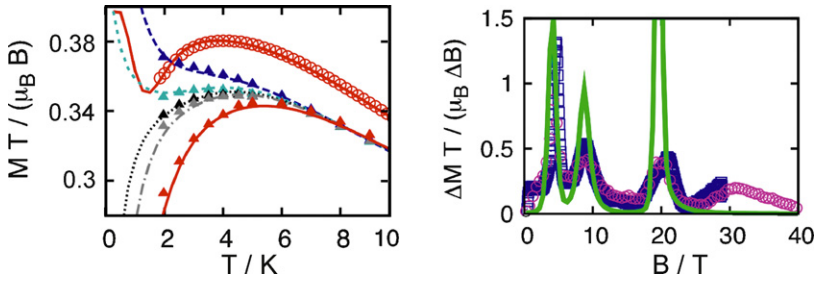

Fig. 6. (Left panel) Experimental data of the magnetic susceptibility of $\{Ni_4Mo_{12}\}$ for batch 1 at $B = 0.5$ T (open circles) and for batch 2 at $B = 0.5$, 3.5, 3.8, 4.2, 5.0 T red, grey, black, turquoise, blue triangles). The theoretical results are given by curves. The panel on the right hand side exhibits the differential magnetization as function of applied field for $T = 0.4$ K. Experimental data are given by symbols, whereas theoretical fits are given by the solid curve. Taken from Ref. [33a,b].

Heisenberg model from the Hubbard model, one usually neglects higher order terms beyond the simple Heisenberg exchange. Considering the next order results in terms that are of generalized biquadratic form. A detailed understanding of the physical origin of such terms requires a thorough investigation on how J^{biq}_{klmn} depends on the Hesse matrix in the case of phonons, or on the hopping parameters and on-site repulsion terms in the Hubbard model. It is well conceivable that both sources are present in a molecule.

The third term in Eq. (2) models the single ion anisotropy of Ni by means of an easy/hard axis along the local direction given by $\vec{e}_k$. The last term (Zeeman term) reflects the interaction with the applied magnetic field. We assume an isotropic g tensor. If the symmetry is reduced from tetrahedral symmetry, the Dzyaloshinskii–Moriya interaction could also contribute [33a,b].

Several good fits can be obtained using Hamitonian (2), as shown in Figs. 6 and 7 for one example (for numerical details see also Ref. [33c]). Here reasonable values are assumed for the impurity content and for the parameters of the Hamiltonian [33a,b]. While the low-field susceptibility is well described, the magnetization is modeled only poorly (Fig. 6). Fig. 7 demonstates that also the available EPR data can be nicely reproduced. The fit needs 18 parameters (given in Ref. [33a,b]) among which we would like to mention $g = 2.223$, the isotropic exchange $J/k_B = -3.28, \ldots, -3.37$ K, the biquadratic exchange of up to 1.31 K as well as local anisotropy tensors of about 2.2 K. For single observables even more accurate fits can indeed be obtained [34], but not for the combined set of experimental data.

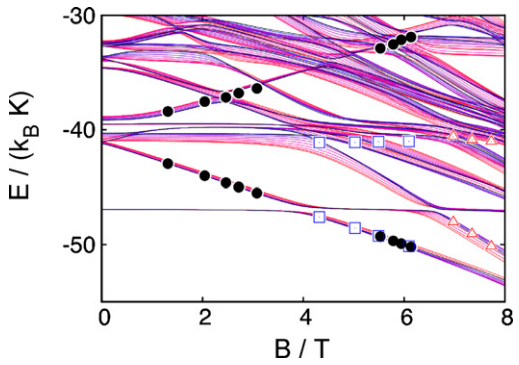

Fig. 7. Energy eigenvalues of Hamiltonian (2) with the parameters used for Fig. 6 for various orientations (curves) as well as observed EPR transitions (superimposed symbols). Taken from Ref. [33a,b].

The persistent discrepancy in modeling the magnetization indicates that some basic mechanisms are not yet implemented despite the large number of parameters. In order to uncover these effects and gain deeper insight, the existing scenarios have to be better understood first. The origin of the generalized biquadratic terms seems to be crucial since they have a major influence on the magnetization curve. The failure to describe the fourth peak in the right panel of Fig. 6 results from the necessity to assume large biquadratic terms. To this end additional investigations are indispensable, among them infrared measurements as well as X-ray spectroscopy under high fields. Both experiments are underway.

4. Metal (Fe^{III}, V^{IV}) oxide clusters in the cavity of the cyclic $\{P_8W_{48}\}$ polytungstate

4.1. $[P_8W_{48}O_{184}Fe_{16}(OH)_{28}(H_2O)_4]^{20-}$ $\{Fe_{16}\}$

Although the crown-shaped tungstophosphate $[H_7P_8W_{48}O_{184}]^{33-}$ $\{P_8W_{48}\}$ has been known for more than 20 years [35], only recently first examples of metal-containing derivatives have been reported. Pope's group prepared a lanthanide derivative, $\{Ln_4(H_2O)_{28}[K\subset P_8W_{48}O_{184}\ (H_4W_4O_{12})_2Ln_2(H_2O)_{10}]^{13-}\}_x$ (Ln = La, Ce, Pr, Nd) [36], Kortz and coworkers isolated the first transition metal derivative [37], the 20-copper(II) containing $[Cu_{20}Cl(OH)_{24}(H_2O)_{12}(P_8W_{48}O_{184})]^{25-}$ (see also the report on the Cu_{20}-azide derivative $[P_8W_{48}O_{184}Cu_{20}(N_3)_6$

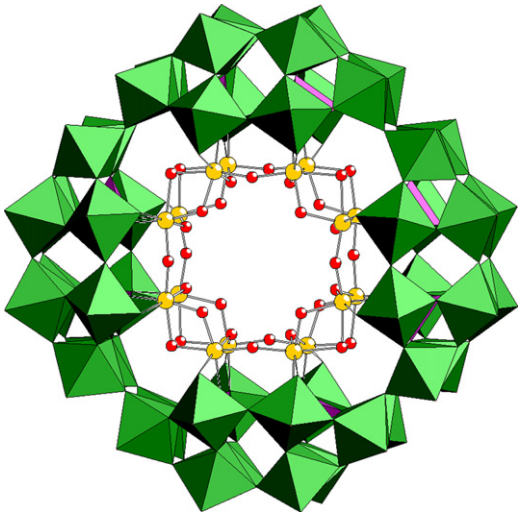

Fig. 8. Top view of $\{Fe_{16}\}$ emphasizing the connectivity of the central $\{Fe_{16}(OH)_{28}(H_2O)_4\}^{20+}$ cluster. Color code: Fe (brown), O (red), PO_4 tetrahedra (pink), WO_6 octahedra (green). Taken from Ref. [41].

$(OH)_{18}]^{24-}$ [38]), while Müller et al. discovered $[K_8 \subset \{P_8W_{48}O_{184}\}\{V^V_4V^{IV}_2O_{12}(H_2O)_2\}_2]^{24-}$ $\{V_{12}\}$ containing two cationic V_6 type mixed-valence clusters and formed by an unprecedented nucleation process [39]. In addition the first organometallic derivative of $\{P_8W_{48}\}$ was reported: $\{K(H_2O)\}_3\{Ru(p\text{-cymene})(H_2O)\}_4P_8W_{49}O_{186}(H_2O)_2]^{27-}$ [40]. Very recently the iron(III) derivative $[P_8W_{48}O_{184}Fe_{16}(OH)_{28}(H_2O)_4]^{20-}$ $\{Fe_{16}\}$ was synthesized and identified independently in Bremen and Bielefeld [41]. It was isolated as the mixed cation salt $Li_4K_{16}[P_8W_{48}O_{184}Fe_{16}(OH)_{28}(H_2O)_4]\bullet 66H_2O\bullet 2KCl$ {LiK-Fe_{16}} and $Na_9K_{11}[P_8W_{48}O_{184}Fe_{16}(OH)_{28}(H_2O)_4]\bullet 100H_2O$ {NaK-Fe_{16}}. The wheel-shaped polyanion $\{Fe_{16}\}$ contains an unprecedented $\{Fe_{16}(OH)_{28}(H_2O)_4\}^{20+}$ cluster in the cavity of $\{P_8W_{48}\}$ with 16 edge- and corner-sharing FeO_6 octahedra being grafted to the inner surface of the tungstophosphate "host" (Figs. 8 and 9).

The molar magnetic susceptibility (χ) and the product χT of {LiK-Fe_{16}} are displayed in Fig. 10 as a function of temperature. When comparing the observed room temperature χT value of 21.9 cm^3 K/mol with the value 70 cm^3 K/mol expected for 16 non-interacting Fe^{III} ions ($s = 5/2$, $g = 2$), it becomes clear that antiferromagnetic interactions play a dominant role in $\{Fe_{16}\}$. At 1.8 K, a χT value of 3.3 cm^3 K/mol suggests that the ground state is $S = 2$ (expected is 3 cm^3 K/mol with $g = 2$).

The highly symmetric magnetic cluster $\{Fe_{16}(OH)_{28}(H_2O)_4\}^{20+}$ incorporated in $\{Fe_{16}\}$ is composed of 16 equivalent Fe^{III} centers (Fig. 8). The three types of Fe–O–Fe bridges (Fig. 11) require three distinct exchange coupling constants J_1 (e.g. Fe1–O1Fe–Fe3), J_2 (e.g. Fe1–O14F/O14G–Fe4) and J_3 (e.g. Fe2–O24F–Fe4); the interplay between them determines the ground state of {LiK-Fe_{16}}. The presence of 163,112,472,594 spin states with a total spin S ranging from 0 to 40 renders the full analysis of the magnetic susceptibility data of {LiK-Fe_{16}} complicated; these details are beyond the scope of the present review. However, when the Fe–O bond distances and Fe–O–Fe bond angles of $\{Fe_{16}\}$ are compared with the literature values for μ_2-hydroxo bridged Fe^{III} dimers and oligomers, the magnitude of J_1, J_2 and J_3 should be in the range of 20–25 cm^{-1} [42]. The exchange couplings are suggested to be of the same magnitude, which results in closely spaced spin levels; hence the assignment of the ground state to $S = 2$ is only tentative. Although our hypothesis is supported by the absence of a plateau at around 3.3 cm^3 K/mol in the χT profile, susceptibility measurements below 1.8 K are needed for confirmation.

The normalized magnetization $M/N_A\mu_B$ of {LiK-Fe_{16}} as a function of external field H is plotted in Fig. 12 for various temperatures. For the lowest temperature $T = 1.8$ K, $M/N_A\mu_B$ tends to approach 4 as the field increases to 7 T, as expected for an $S = 2$ spin system with $g = 2$. As the temperature rises from 1.8 to 20 K, the magnetization decreases, which might be explained by the expected H/T dependence of the magnetization [43].

In a further attempt to understand the magnetism of polyanion $\{Fe_{16}\}$, electron paramagnetic resonance (EPR) spectra were collected for various frequencies (9.6–319.2 GHz) and temperatures (5–300 K) for a powder sample of {LiK-Fe_{16}}. For all frequencies of this investigation, at room temperature only one broad peak ($\Delta H_{pp} = 70 \pm 3$ mT) is observed at $g = 2.002 \pm 0.001$ (Fig. 13).

Fig. 14 presents the temperature dependence of X-band (~9.6 GHz) and ~319 GHz spectra at some selected temperatures. From these data at least three features are evident: (a) the signal intensity strongly decreases as the temperature is reduced, (b) the signal broadens at lower temperatures and (c) the main peak does not exhibit any additional splitting. The intensity decrease is consistent with the similar trend in magnetic susceptibility (Fig. 10), and can thus be attributed to the population of states with smaller S values at lower temperatures. On the other hand, the signal broadening could also be due to dipolar broadening and/or shorter relaxation times. The lack of any fine structure at any frequency or temperature renders it meaningless to derive any conclusions about the single-ion anisotropy of the overall S value. It should be noted: (a) the low temperature peak indicated by '*' in the X-band spectra (Fig. 14, left panel) is an Fe^{III} impurity signal from the sample and corresponds to g ~4.3. (b) The small remnant signal observed at 319.2 GHz (Fig. 14, right panel) is attributed to a minor impurity (with $g \sim 2$) in the system and is not considered significant to the overall focus of the present study.

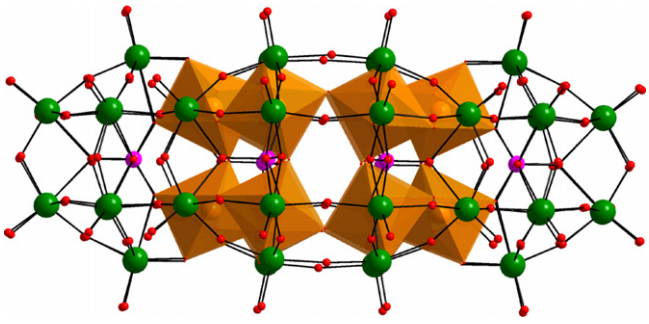

Fig. 9. Side view of $\{Fe_{16}\}$ emphasizing the FeO_6 octahedra (brown) in polyhedral representation. Color code: W (green), O (red), P (pink). Taken from Ref. [41].

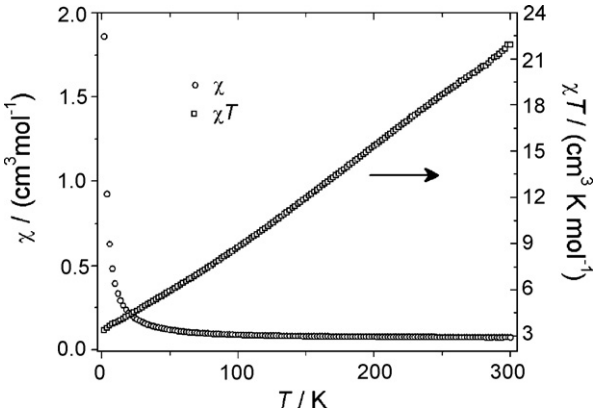

Fig. 10. Magnetic susceptibility plotted as χ (○), χT (□) vs. T for {LiK-Fe_{16}} powder. Taken from Ref. [41].

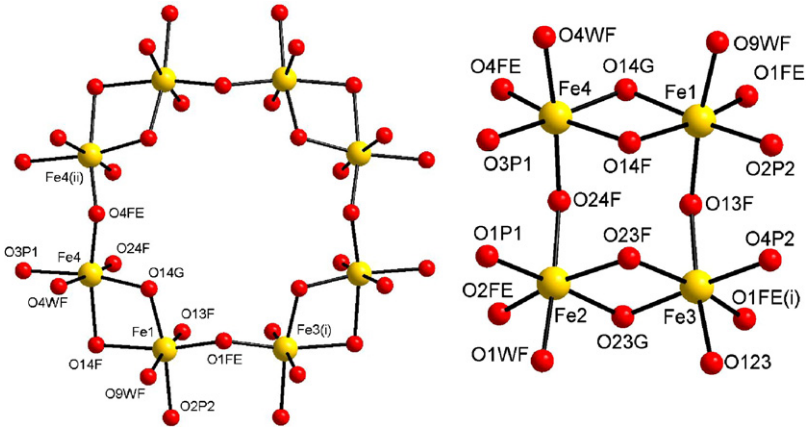

Fig. 11. Left: Ball-and-stick view of a segment of $\{Fe_{16}\}$. Right: Side view including four independent Fe^{III} centers. Oxygen atoms O9WF, O4WF, O1WF, and O123 bridge to atoms W9, W4, W1, and W12, respectively. The atoms O1P1, O3P1, O2P2, and O4P2 bridge to atoms P1 and P2. Taken from Ref. [41].

4.2. $[K_8 \subset \{P_8W_{48}O_{184}\}\{V^V{}_4V^{IV}{}_2O_{12}(H_2O)_2\}_2]^{24-}$ $\{V_{12}\}$

The versatility of the $\{P_8W_{48}\}$ wheel becomes clear from the variety of clusters prepared by nucleation processes in its cavity. Employed metals range from early to late first row transition metal ions, including lanthanides. The nuclearity of the generated clusters ranges from 4 to 20. $\{P_8W_{48}\}$ reacts with vanadyl sulfate in aqueous solution and forms $[K_8 \subset \{P_8W_{48}O_{184}\}\{V^V{}_4V^{IV}{}_2O_{12}(H_2O)_2\}_2]^{24-}$ $\{V_{12}\}$ where two V_6 aggregates cap the cavity of $\{P_8W_{48}\}$ [39]. Each of the capping units consists of two octahedral V^{IV} centers and four tetrahedral V^V centers (see Fig. 15).

Electronic absorption spectra of $\{V_{12}\}$ give evidence for a Robin–Day class I mixed valence compound with only very weak direct electronic interaction among the vanadium sites. However, the same electronic absorption spectra (class II mixed valence) point towards significant electronic interactions between the V^{IV} and the W^{VI} ions.

Magnetic measurements indicate that the paramagnetic V^{IV} centers interact weakly. The room temperature χT value of 1.35 $cm^3\,K\,mol^{-1}$ (Fig. 16) agrees with four V^{IV} ions being present. The decrease in the χT value below 50 K and the $\theta = -1.8 \pm 0.2$ K clearly demonstrate the presence of antiferromagnetic exchange interactions. This is surprising, since the two V^{IV} centers on the same V_6 aggregate can interact only through a V^{IV}(oct)–O–V^V(tet)–O–V^V(tet)–O–V^{IV}(oct) superexchange pathway which is not very effective for the V^{IV} and V^V centers. On the other hand, the V^{IV} sites on different V_6 aggregates are linked by multiple V^{IV}–O–W^{VI}–O–W^{VI}–O–W^{VI}–O–W^{VI}–O–V^{IV} pathways, which are probably more efficient in transmitting magnetic information, given the V^{IV}–W^{VI} class II mixed valency, i.e. larger electronic interaction. This long exchange pathway explains the weak interaction.

X-Band EPR spectroscopy corroborates the proposed presence of two exchange coupled pairs of V^{IV} ions. The spectra displayed in Fig. 17 show more lines than expected for a single vanadyl ion including hyperfine splitting. However, very good simulations can be achieved for a triplet state coupled to two vanadium nuclei. The obtained spin Hamiltonian parameters are $g_{||} = 1.93$, $g_{\perp} = 1.93$, $A_{||} = 75 \times 10^{-4}\,cm^{-1}$, $A_{\perp} = 30 \times 10^{-4}\,cm^{-1}$. The accuracy of the obtained parameters is limited by line-broadening, which may be caused by an increase in spin-lattice relaxation due to interactions between the two exchange coupled pairs of ions within the same molecule.

Because of the antiferromagnetic exchange coupling this triplet state is the excited state, but given the relatively modest exchange interaction this triplet state is already appreciably populated at the lowest temperatures reached in experiment.

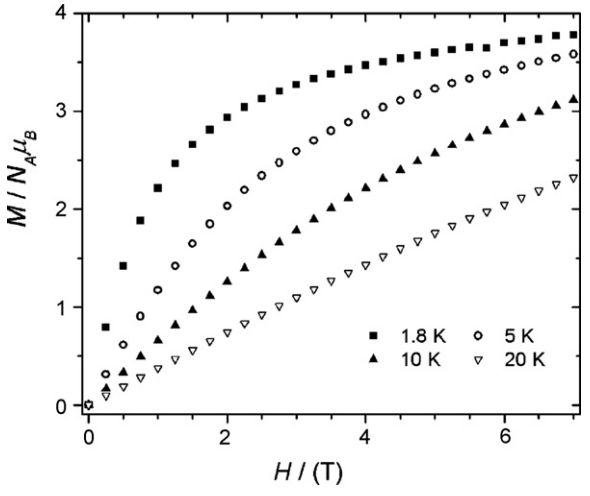

Fig. 12. Normalized magnetization ($M/N_A\mu_B$) as a function of magnetic field H for $\{LiK\text{-}Fe_{16}\}$ powder plotted for various temperatures as indicated. Taken from Ref. [41].

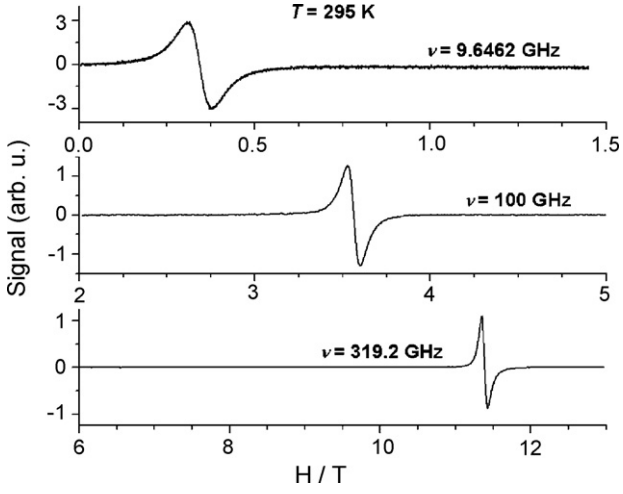

Fig. 13. Room temperature powder EPR spectra of $\{LiK\text{-}Fe_{16}\}$ for 9.65, 100 and 319.2 GHz, respectively. Only one broad peak at $g = 2.002$ is observed for all experimental frequencies. Taken from Ref. [41].

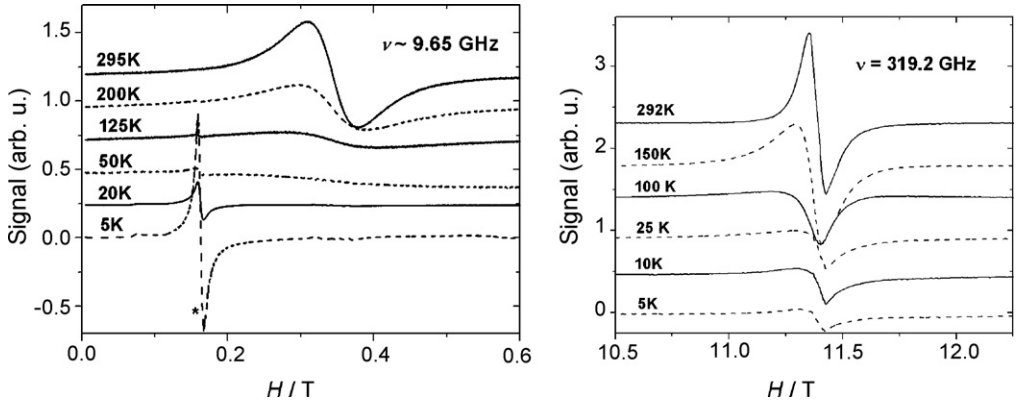

Fig. 14. Temperature dependence of EPR spectra on {LiK-Fe_{16}} powder at ~9.65 GHz (left panel) and 319.2 GHz (right panel). The steady decrease of the signal intensity with decreasing temperature indicates the presence of excited states. The peak at ~0.16 T indicated by '*' in the X-band spectra is from an Fe^{III} impurity in the sample. Taken from Ref. [41].

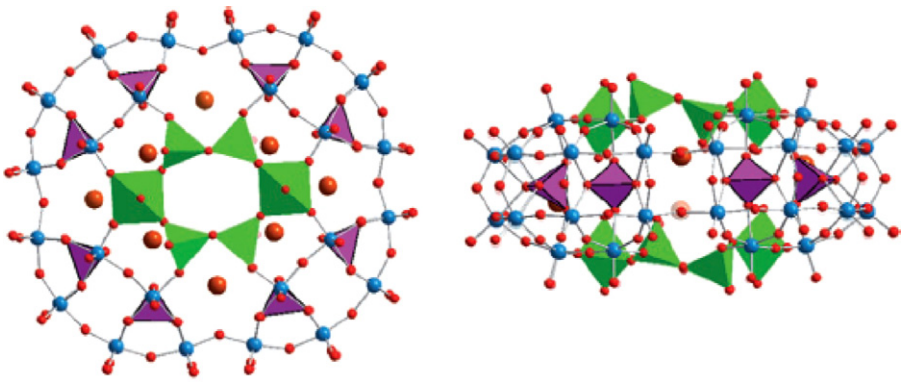

Fig. 15. Two views of the structure of {V_{12}} which show the capping V_6 groups and the positions of the K cations within the cavity. Color code: W (blue), O (small red spheres), K (large brown-red spheres), PO_4 (pink), VO_n (green). Taken from Ref. [39].

5. Magnetic properties of the {Cu_3} spin triangle in {$Cu_3X^{III}_2W_{18}$} (X = As, Sb)

The copper(II)-substituted polyoxotungstates $[Cu_3Na_3(H_2O)_9(\alpha\text{-}XW_9O_{33})_2]^{9-}$ (X = As^{III}, {Cu_3As}; Sb^{III}, {Cu_3Sb}) have a sandwich-type structure with D_{3h} symmetry, where {Cu_3} resides in the central plane covered by two (α-XW_9O_{33}) Keggin subunits as displayed in Fig. 18a [1e,12,44]. Spin exchange coupling between the Cu^{II} ions occurs in an indirect way via two W and three O atoms of each (XW_9O_{33}) fragment. This makes it possible to modify the magnitude of the spin interaction by changing the diamagnetic heteroatom X. Fig. 18b and c depicts the spin topology of {Cu_3X}. For {Cu_3As}, the distances between the copper ions are Cu1···Cu2 = 4.696 Å and Cu2···Cu2 = 4.689 Å, while for {Cu_3Sb} the respective distances increase slightly to Cu1···Cu2 = 4.871 Å and Cu2···Cu2 = 4.772 Å, respectively. The reason for that is most likely the difference of lone pair–lone pair interactions between the two X hetero atoms. Since Sb has a larger size than As, the lone pair interactions between Sb become stronger, leading to a larger separation of the copper centers.

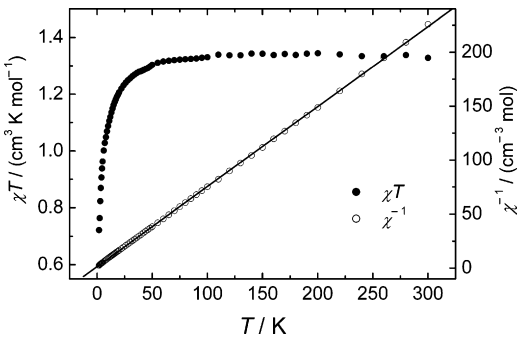

Fig. 16. Susceptibility temperature product χT (() and inverse susceptibility χ^{-1} (() as a function of temperature T for {V_{12}}. Taken from Ref. [39].

In Fig. 19, the magnetization of {Cu_3X} is plotted as a function of magnetic field. The data are taken at 0.4 K for H oriented in the plane comprising the spin triangle [12b]. The measurements were performed in a full cycle sweep at a time scale of about 5 ms. Note that the saturation magnetization is renormalized by gS, where the g-factor was determined by electron spin resonance. In the upward sweep ($A \rightarrow B$), the magnetization of {Cu_3As} first increases to $1\,gS\mu_B$, followed by the step of $2.3\,gS\mu_B$, and finally approaches the saturation value of $3\,gS\mu_B$ in a high magnetic field of 12 T. In the down sweep ($B \rightarrow C$), the magnetization drops sharply from $3\,gS\mu_B$ to $1\,gS\mu_B$ and from $1\,gS\mu_B$ to zero, respectively, before it reverses direction. The former $2\,gS\mu_B$ step originates from the level crossing between $S = 1/2$ and 3/2 states. The latter $1\,gS\mu_B$ one is related to a splitting of the $S = 1/2$ state at zero field (see below for more details). The $1.3\,gS\mu_B$ step seen in the upward sweep cannot be understood within a simple energy level scheme of a spin triangle. The contrasting magnetization between the up and down sweeps leads to a pronounced hysteresis loop. In the negative field, the hysteresis behaviour nearly disappears. The magnetization of the negative field is similar to the magnetization which is seen in the down sweep of the positive field. We stress that the hysteresis loop is not associated with an energy barrier since Cu^{II} has no single ion anisotropy and the Cu^{II} triangle is coupled antiferro-

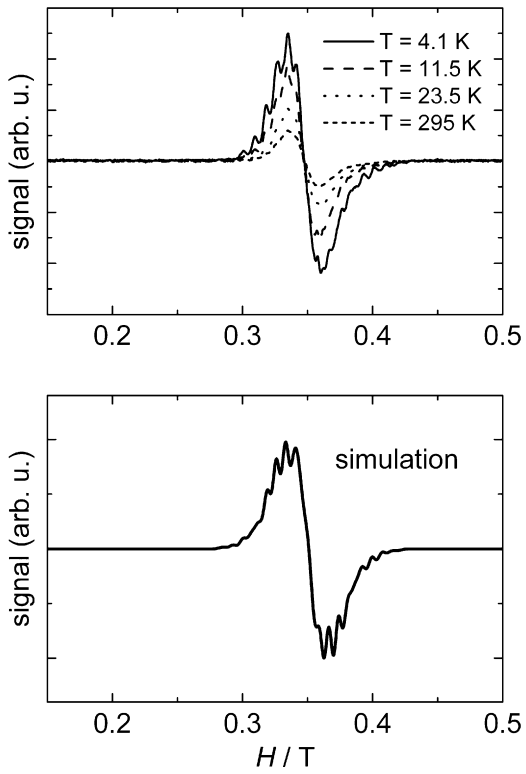

Fig. 17. Upper panel: EPR spectrum of $\{V_{12}\}$. The experimental data are taken at various temperatures, but the hyperfine splitting is only resolved for 4.1 K. Lower panel: simulation with g and A parameters from Table 1 in Ref. [55], $D = 0.008\ cm^{-1}$, and linewidths of 60 G. Taken from Ref. [39].

magnetically. Rather, the asymmetric magnetization through the positive and negative fields implies that the magnetization reversal dynamics is slow on the time scale of the pulsed field sweep rate.

Upon switching to $\{Cu_3Sb\}$, the magnetization steps become less sharp in comparison to $\{Cu_3As\}$. In addition, the magnetization curve looks more symmetric between the positive and negative fields. This is mainly due to the smearing of the $2.3\ gS\mu_B$ step in the positive field and the appearance of the small step in the negative field between −5 and −7 T, which is absent in $\{Cu_3As\}$. The dependence of the magnetization on the heteroatom X suggests that the dynamic magnetization processes are distinctly different in the two compounds.

The spin-Hamiltonian parameters obtained from the EPR of these compounds [26,27] were in contrast to those of an earlier reported Cu_3 compound [45]. This reemphasizes nicely that POMs are ideal examples for studying on a molecular level the nature of the exchange interactions between transition metal ions. The diamagnetic polytungstate fragments usually encapsulate and isolate the magnetic cluster, so that intermolecular coupling and structural distorsions become negligible.

We have also prepared a tetra-copper(II) containing sandwich-type tungstogermanate $[Cu_4(H_2O)_2(GeW_9O_{34})_2]^{12-}$, which was characterized in detail by magnetic and EPR techniques and serves as a model coupled 4-spin system [46].

6. A model five-spin frustrated $\{Cu_5\}$ cluster in $\{Cu_5Si_2W_{18}\}$

The dimeric polyanion $[Cu_5(OH)_4(H_2O)_2(A\text{-}\alpha\text{-}SiW_9O_{33})_2]^{10-}$ $\{Cu_5\}$ consists of two A-α-$[SiW_9O_{34}]^{10-}$ Keggin moieties that are linked via two adjacent W–O–W bonds and stabilized by a central $\{Cu_5(OH)_4(H_2O)_2\}^{6+}$ fragment, leading to a structure with idealized C_{2v} symmetry (Fig. 20a) [47]. The polyanion $\{Cu_5\}$ is stable over a very wide pH range (pH 1–7), as shown by UV–vis and IR spectroscopy. The structure of $\{Cu_5\}$ can also be visualized as an open Wells-Dawson polyanion $[Si_2W_{18}O_{66}]^{16-}$ (first reported by Hervé and co-workers) [48], which has taken up the cationic copper-oxo cluster $\{Cu_5(OH)_4(H_2O)_2\}^{6+}$. The structural details of this $\{Cu_5(OH)_4(H_2O)_2\}^{6+}$ fragment are of interest (Fig. 20b). Bond valence sum calculations indicate that all bridging oxo groups linking adjacent copper atoms are either mono- or diprotonated [49]. Specifically, oxygen atoms O1CC, OC12, O25C, and O34C are monoprotonated (OH), whereas oxygen atoms O13C and O24C are diprotonated (H_2O). As expected, the octahedral coordination spheres of all copper(II) centers are Jahn-Teller distorted. The equatorial Cu–O distances range from 1.907 to 2.084(13) Å, whereas the axial Cu–O distances are 2.280–2.387(13) Å. The Cu–O–Cu angles of the central $\{Cu_5(OH)_4(H_2O)_2\}^{6+}$ fragment range from 83.6° to 129.3(6)°, and the Cu···Cu separations in $\{Cu_5\}$ range from 3.11 to 3.56 Å. The pentacopper-substituted polyanion $\{Cu_5\}$ is highly interesting for magnetic and EPR studies.

Fig. 21a shows magnetic susceptibility data for $\{Cu_5\}$ as a plot of χT versus T. Upon cooling χT steadily decreases from 1.15 cm^3 K/mol at 300 K to 0.44 cm^3 K/mol at 80 K and slowly saturates to 0.39 cm^3 K/mol as the temperature further decreases to 1.8 K. Comparison of the low-temperature saturation value (0.39 cm^3 K/mol) to the calculated value of 0.41 cm^3 K/mol for $s = 1/2$ and $g = 2.1$ implies that the spin of the ground state is $S = 1/2$.

Following the numbering scheme in Fig. 20b, the isotropic spin-exchange Hamiltonian for $\{Cu_5\}$ can be given as

$$\hat{H}_{exch} = -2[J_{12}\hat{s}_1 \cdot \hat{s}_2 + J_{24}\hat{s}_2 \cdot \hat{s}_4 + J_{34}\hat{s}_3 \cdot \hat{s}_4 + J_{13}\hat{s}_1 \cdot \hat{s}_3 + J_{15}\hat{s}_1 \cdot \hat{s}_5 + J_{25}\hat{s}_2 \cdot \hat{s}_5 + J_{45}\hat{s}_4 \cdot \hat{s}_5 + J_{35}\hat{s}_3 \cdot \hat{s}_5] \quad (3)$$

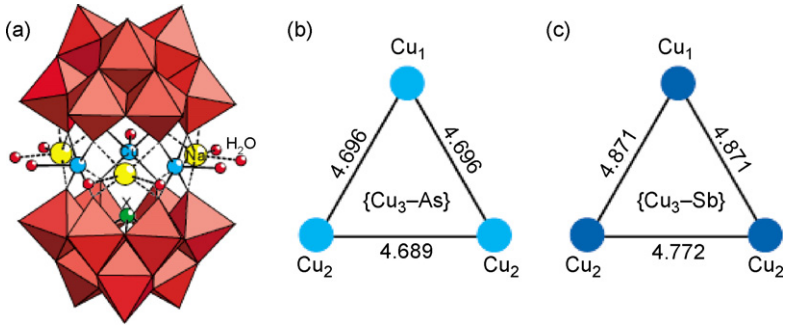

Fig. 18. (a) Combined polyhedral/ball-and-stick representation of $[Cu_3Na_3(H_2O)_9(\alpha\text{-}XW_9O_{33})_2]^{9-}$ (X = As^{III}, Sb^{III}). Color code: Na (yellow), Cu (cyan), X (green), and H_2O (red). The panels (b) and (c) sketch the $\{Cu_3\}$ triangle configuration for $\{Cu_3As\}$ and $\{Cu_3Sb\}$ and show the Cu···Cu distances. Cu_1 and Cu_2 represent two crystallographically inequivalent Cu sites. Taken from Ref. [12b].

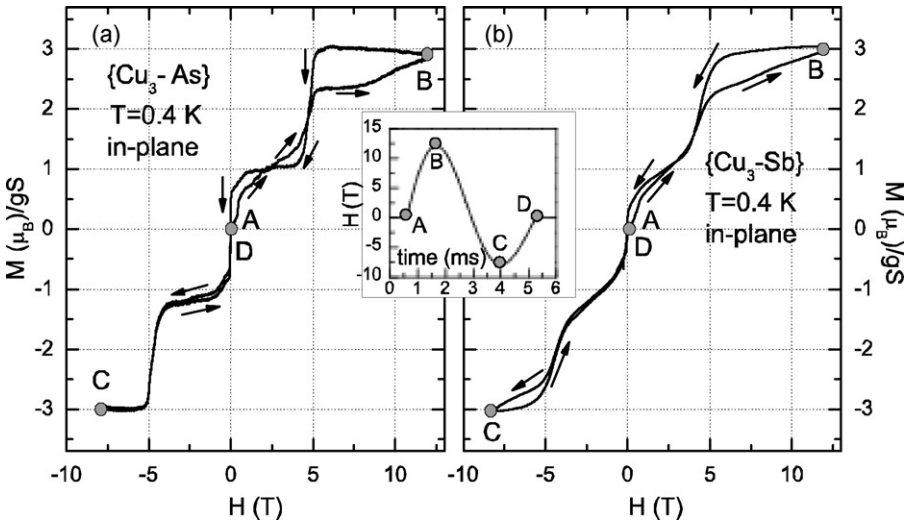

Fig. 19. (a) Magnetization curve vs. magnetic field strength for $\{Cu_3As\}$ at $T = 0.4$ K for H || triangle plane. The saturated magnetization is normalized by gS. Arrows are a guide to sweep directions ($A \rightarrow B \rightarrow C \rightarrow D$). (b) Magnetization of $\{Cu_3Sb\}$ using a pulsed field with the same conditions as (a). The inset shows the time dependence of a pulsed magnetic field. Taken from Ref. [12b].

Considering the C_{2v} symmetry of the pentamer, the above Hamiltonian can be rewritten as

$$\hat{H}_{exch} = -2J_a[\hat{s}_1 \cdot \hat{s}_2 + \hat{s}_3 \cdot \hat{s}_4] - 2J_b[\hat{s}_1 \cdot \hat{s}_3 + \hat{s}_2 \cdot \hat{s}_4] - 2J_c[\hat{s}_1 \cdot \hat{s}_5 + \hat{s}_2 \cdot \hat{s}_5 + \hat{s}_4 \cdot \hat{s}_5 + \hat{s}_3 \cdot \hat{s}_5] \quad (4)$$

where $J_{12} = J_{34} = J_a$, $J_{13} = J_{24} = J_b$, and $J_{15} = J_{25} = J_{35} = J_{45} = J_c$. The Hamiltonian in Eq. (4) gives rise to 10 spin states corresponding to the total spin operator $\hat{S} = \hat{s}_1 + \hat{s}_2 + \hat{s}_3 + \hat{s}_4 + \hat{s}_5$, viz., five doublets ($\hat{S} = 1/2$), four quartets ($\hat{S} = 3/2$), and one sextet ($\hat{S} = 5/2$). The eigenvalues associated with the Hamiltonian in Eq. (4), obtained by solving the 32×32 matrix, are listed in Table 1. The molar magnetic susceptibility expression shown in Eq. (5) was then obtained by substituting the energies of Table 1 in the Heisenberg-Dirac-van Vleck equation [43b].

$$\chi = \left(\frac{N_A g^2 \mu_B^2}{4 k_B T}\right)\left(\frac{A}{B}\right) \quad (5)$$

Here N_A is Avogadro's number, g is the Landé factor, μ_B is the electron Bohr magneton, k_B is the Boltzmann constant, T is the temperature in Kelvin, $A = 35\ \exp(2x + 2y + 5z) + 10\ \exp(2y + 4z) + 10\ \exp(2x + 4z) + 10\ \exp(4z) + 10\ \exp(2x + 2y) + \exp(3z + 2(x^2\text{-}xy + y^2)^{1/2}) + \exp(3z - 2(x^2\text{-}xy + y^2)^{1/2}) + \exp(2y + z) + \exp(2x + z) + \exp(z)$, and $B)\ 3\ \exp(2x + 2y + 5z) + 2\ \exp(2y + 4z) + 2\ \exp(2x + 4z) + 2\ \exp(4z) + 2\ \exp(2x + 2y) + \exp(3z + 2(x^2\text{-}xy + y^2)^{1/2}) + \exp(3z - 2(x^2\text{-}xy + y^2)^{1/2}) + \exp(2y + z) + \exp(2x + z) + \exp(z)$, with $x = J_a/k_BT$, $y = J_b/k_BT$, and $z = J_c/k_BT$.

The experimental data were fitted by Eq. (5) with g, J_a, J_b, and J_c as parameters. As shown in Fig. 21a, the least-squares fit is quite satisfactory and yields $J_a = -51 \pm 6\ cm^{-1}$, $J_b = -104 \pm 1\ cm^{-1}$, $J_c = -55 \pm 3\ cm^{-1}$, and $g = 2.035 \pm 0.002$. The spin-state spectrum along with the energies relative to the ground state is shown in Fig. 21b. The doublet ground state is well separated from the first excited state ($S = 1/2$) by approximately $70\ cm^{-1}$ ($\sim$101 K), which is consistent with our EPR results.

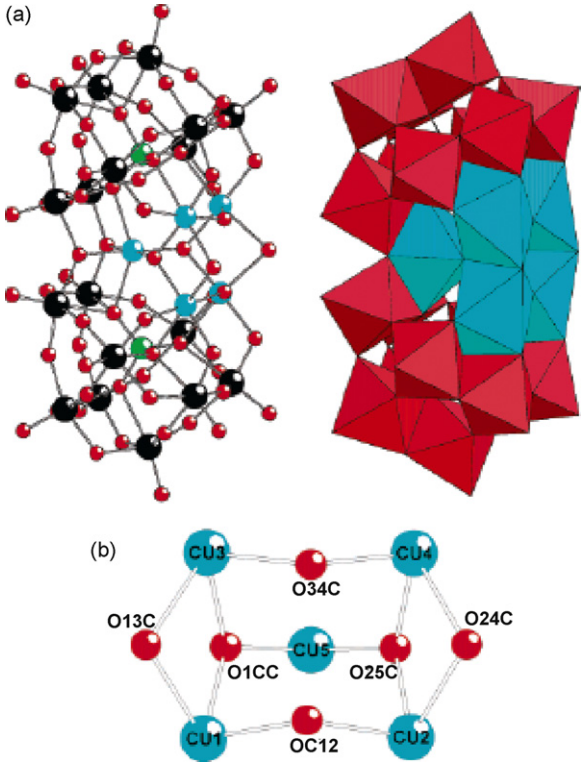

Fig. 20. (a) Ball-and-stick (left) and polyhedral (right) representations of $\{Cu_5\}$. The color code is as follows: Cu (turquoise), W (black), Si (green), O (red). (b) Ball-and-stick representation of the central $\{Cu_5(OH)_4(H_2O)_2\}^{6+}$ fragment of $\{Cu_5\}$. Taken from Ref. [47a].

Table 1
Eigenvalues associated with the spin-exchange Hamiltonian for $\{Cu_5\}$. Taken from Ref. [47b].

n	S	E(S)
1	5/2	$-J_a - J_b - 2J_c$
2	3/2	$J_a - J_b - J_c$
3	3/2	$-J_a + J_b - J_c$
4	3/2	$J_a + J_b - J_c$
5	3/2	$-J_a - J_a + 3J_c$
6	1/2	$J_a + J_b - 2\sqrt{J_a^2 - J_aJ_b + J_b^2}$
7	1/2	$J_a + J_b + 2\sqrt{J_a^2 - J_aJ_b + J_b^2}$
8	1/2	$J_a - J_b + 2J_c$
9	1/2	$-J_a + J_b + 2J_c$
10	1/2	$J_a + J_b + 2J_c$

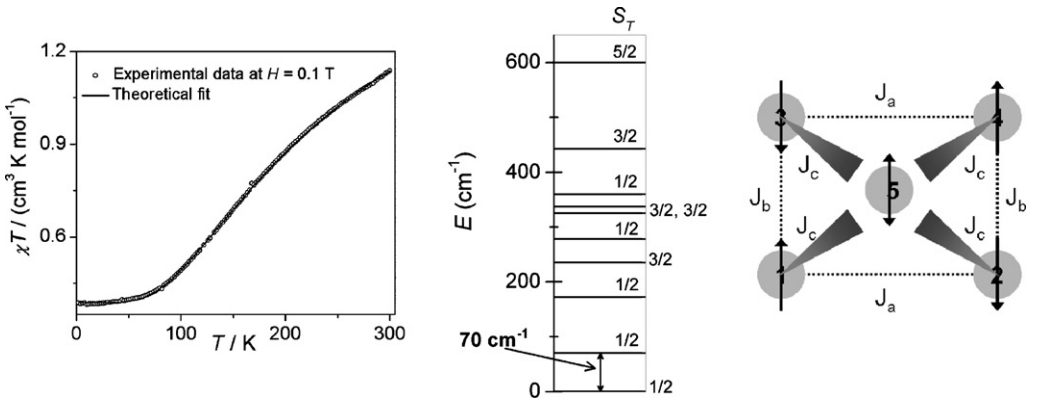

Fig. 21. (Left) Plot of χT vs. T for $\{Cu_5\}$ at $H = 0.1$ T. The solid line is a theoretical fit to Eq. (5). See text for details. (Middle) Calculated spin-state energies, relative to the ground state of $\{Cu_5\}$. (Right) Spin-exchange coupling in the $\{Cu_5(OH)_4(H_2O)_2\}^{6+}$ core of $\{Cu_5\}$, where the numbering corresponds to that of Fig. 20b. Up and down arrows on the apical Cu^{II} ion (Cu_5) represent the spin frustration experienced by it. Taken from Ref. [47b].

Table 2
Bond distances (Å) and angles (°) for the central $\{Cu_5(OH)_4(H_2O)_2\}^{6+}$ fragment in $\{Cu_5\}$. Taken from Ref. [47b].

	Cu1	Cu2	Cu3	Cu4	Cu5	Cu–O–Cu
O13C	2.28(1)		2.37(1)			85.0(5)
OC12	1.95(1)	1.92(1)				128.4(6)
O24C		2.30(2)		2.37(2)		83.6(5)
O34C			1.95(1)	1.91(1)		129.3(7)
O1CC	2.09(1)		2.02(1)		1.96(1)	100.2(5) 122.6(6) 123.1(6)
O25C		2.05(1)		2.03(1)	1.98(1)	99.5(5) 122.8(6) 123.1(6)

The observed J values can be correlated with the molecular structure by considering the available exchange pathways between the Cu^{II} ions (see Table 2 for bond lengths and angles). Cu1(3)···Cu2(4) are connected via a μ_2-OH with a bridging angle of about 129°, and Cu1(2,3,4)···Cu5 are connected via a μ_3-OH with a bridging angle of about 123°, thus giving rise to antiferromagnetic exchange interactions ($J_a = -51 \pm 6\,cm^{-1}$ and $J_c = -55 \pm 3\,cm^{-1}$, respectively). On the other hand, Cu1(2)···Cu3(4) are connected via both a μ_2-OH_2 and a μ_3-OH with bridging angles of about 84° and 100°, respectively, and therefore can interact either ferromagnetically or antiferromagnetically [50]. Considering that the Cu–O bond length (~2.05 Å) is shorter along the μ_3-OH bridge than the μ_2-OH_2 (~2.33 Å) and the fact that Cu1-(2,3,4)···Cu5 interact antiferromagnetically via the same μ_3-OH bridge, we believe that Cu1(2)···Cu3(4) are antiferromagnetically coupled via the μ_3-OH bridge ($J_b = -104 \pm 1\,cm^{-1}$). The magnetic exchange parameters obtained in the present study are consistent with other pentanuclear Cu^{II} complexes reported in the literature [51]. The spin-exchange coupling scheme is shown in Fig. 21c, where Cu1, Cu2, Cu3, and Cu4 are in the plane and Cu5 is projecting out of the plane. The dominant antiferromagnetic exchange interactions in the plane align the spins antiparallel, thus making $\{Cu_5\}$ a spin-frustrated center.

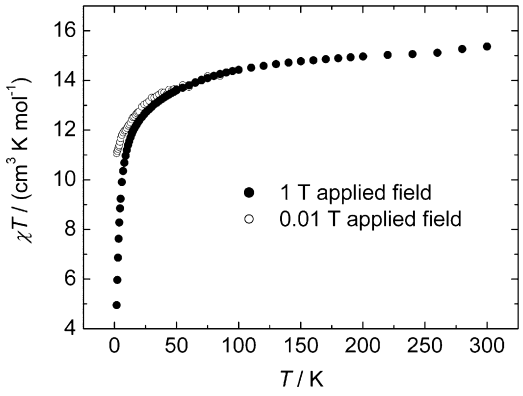

Fig. 22. Susceptibility–temperature product as a function of temperature measured at a static field of 1 T ((dots) and 0.01 T ((). Taken from Ref. [2a].

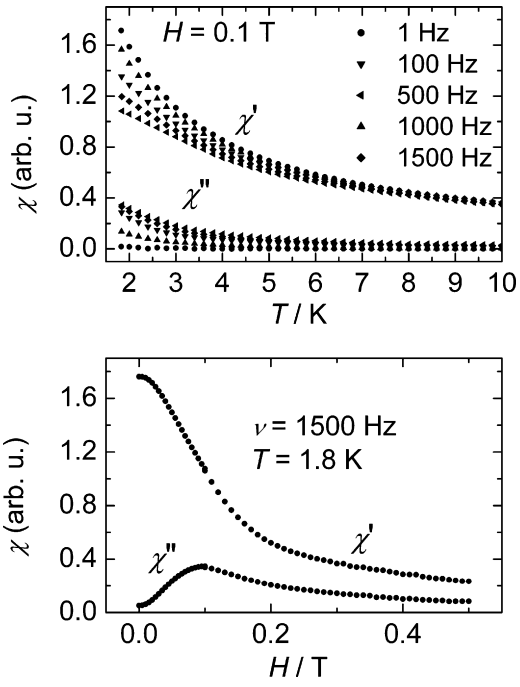

Fig. 23. (Upper panel) Real and imaginary parts of the temperature-dependent ac susceptibility measured at different frequencies as indicated with a static field of 0.1 T. (Lower panel) Field dependence of the real and imaginary parts of the susceptibility; the data are taken at $T = 1.8$ K and a frequency of 1.5 kHz. Taken from Ref. [2a].

7. Lanthanide ions M^{III} in $\{V^{IV}_2M^{III}\}\{As^{III}W_9O_{33}\}_2$ sandwich type clusters

Many complexes in which three transition metal ions are sandwiched between two lacunary (α-$As^{III}W_9O_{33}$) units have been reported [44a,c,52]. None of these derivatives feature lanthanide ions. Recently, however, a mixed transition metal-lanthanide derivative was reported that contains the central unit $\{Dy^{III}V^{IV}_2\}$ and two ($As^{III}W_9O_{33}$) moieties [2a]. The magnetic moment at room temperature (Fig. 22) corresponds well to that expected for the three uncoupled paramagnetic ions. Although the magnetic moment decreases towards very low temperatures, this is likely an effect of the crystal field splitting of the ground multiplet of the dysprosium ion. This is supported by magnetic measurements on the derivative with the diamagnetic La^{III} ion [53], which shows negligible exchange interactions between the two vanadyl ions. Interestingly, the molecule shows slow relaxation of the magnetization in applied dc fields, as evidenced by the ac susceptibility measurements in Fig. 23. In view of the rather weak exchange interactions, this slow relaxation is probably due to the crystal field splitting of the total angular momentum $J = 15/2$ ground multiplet of the dysprosium ion. The absence of slow relaxation in zero applied dc field is likely to be due to quantum tunneling of the magnetization, allowed by hyperfine interactions, as was shown for bis-phthalocyanine complexes of dysprosium [54]. Recently, a second example of slow relaxation in a rare earth containing POM was reported [2c].

8. Conclusions

POMs display an astounding range of paramagnetic derivatives, from early to late transition metals and including lanthanide ions. The reason for the importance of POM chemistry is the fact that paramagnetic centers can be (deliberately) embedded in a large variety of different structure-determining diamagnetic POM frameworks while a multitude of physical phenomena can be studied, such as slow magnetization dynamics and quantum tunneling of the magnetization. Regarding properties: as it is considered a tremendous challenge in the scientific community to find a way to use molecular magnets for quantum information processing we could refer to a Highlight of R.E.P. Winpenny who claims in the graphical abstract of Ref. [55]: "Recent observations using pulsed EPR spectroscopy suggest that it could be possible to use magnetic molecules such as the $\{V_{15}\}$ POM cage in quantum information processing (QIP). Controlled interactions of cage complexes with an $S = 1/2$ ground state, acting as qubits, could allow QIP." (For further related theoretical proposals for the exact handling of $\{V_{15}\}$ see papers cited in Ref. [55].) In this context it is important to note that the control of complex coherent spin states of the molecular magnets – in which exchange interactions can be tuned by well defined chemical changes of the metal cluster ligand spheres – could finally enable to circumvent the 'roadblock' of decoherence.

Acknowledgements

The authors acknowledge generous financial support by the DFG under contracts KO-2288/3, SCHN 615/8, DR-228/19, MU 283/33 and by NSF-DMR under grant # 0506946 and the State of Florida and the NSF Cooperative Agreement No. DMR 0654118 for work at NHMFL.

We thank our colleagues who were involved in the writing of our cited original papers, such as Kwang-Yong Choi, Boris Gorshunov, Bernt Krebs, Marshall Luban, Alexander Mukhin, Sarita Nellutla, Hiroyuki Nojiri, Michael Pope, and Boris Tsukerblat.

Furthermore we thank our coworkers for the enthusiasm and significant contributions they provided, i.e. Li-Hua Bi, Mirko Brüger, Fadi El Hallak, Firasat Hussain, Nadeschda Kirchner, Mechtild Läge, Sib Sankar Mal, Alice Merca, Christoph Schlegel, Filipa L. Sousa, Ashley C. Stowe, Ana Maria Todea, Johan van Tol, and Suriyakan Vongtragool.

References

[1] (a) M.T. Pope, A. Müller, Angew. Chem. Int. Ed. Engl. 30 (1991) 34;
(b) A. Müller, S. Roy, in: C.N.R. Rao, A. Müller, A.K. Cheetham (Eds.), The Chemistry of Nanomaterials: Synthesis, Properties and Applications, Wiley-VCH, Weinheim, 2004, p. 452;
(c) D. Gatteschi, R. Sessoli, J. Villain, Molecular Nanomagnets, Oxford University Press, Oxford, 2006;
(d) A. Müller, F. Peters, M.T. Pope, D. Gatteschi, Chem. Rev. 98 (1998) 239;
(e) J.M. Clemente-Juan, E. Coronado, Coord. Chem. Rev. 193–195 (1999) 361;
(f) P. Day, E. Coronado, in: J.S. Miller, M. Drillon (Eds.), Magnetism: Molecules to Materials V, Wiley-VCH Verlag GmbH &Co, Weinheim, Germany, 2005, p. 105;
(g) D. Gatteschi, R. Sessoli, A. Müller, P. Kögerler, in: M.T. Pope, A. Müller (Eds.), Polyoxometalate Chemistry: From Topology via Self-Assembly to Applications, Kluwer, Dordrecht, 2001, p. 319;
(h) M.T. Pope, A. Müller (Eds.), Polyoxometalate Chemistry: From Topology Via Self-Assembly to Applications, Kluwer, Dordrecht, The Netherlands, 2001;
(i) M.T. Pope, T. Yamase (Eds.), Polyoxometalate Chemistry for Nanocomposite Design, Kluwer, Dordrecht, The Netherlands, 2002;
(j) J.J. Borrás-Almenar, E. Coronado, A. Müller, M.T. Pope (Eds.), Polyoxometalate Molecular Science, Kluwer, Dordrecht, The Netherlands, 2003;
(k) M.T. Pope, in: J.A. McCleverty, T.J. Meyer (Eds.), Comprehensive Coordination Chemistry II, Elsevier Ltd, Oxford, UK, 2004;
(l) M.T. Pope, Heteropoly and Isopoly Oxometalates, Springer-Verlag, Berlin, 1983.

[2] (a) A. Merca, A. Müller, J. van Slageren, M. Lage, B. Krebs, J. Clust. Sci. 18 (2007) 711;
(b) C. Ritchie, A. Ferguson, H. Nojiri, H.N. Miras, Y.F. Song, D.L. Long, E. Burkholder, M. Murrie, P. Kögerler, E.K. Brechin, L. Cronin, Angew. Chem. Int. Ed. 47 (2008) 5609;
(c) M.A. Al Damen, J.M. Clemente-Juan, E. Coronado, C. Martí-Gastaldo, A. Gaita-Ariño, J. Am. Chem. Soc. 130 (2008) 8874.

[3] A. Müller, J. Döring, Angew. Chem. Int. Ed. Engl. 27 (1988) 1721.

[4] (a) D. Gatteschi, L. Pardi, A.L. Barra, A. Müller, J. Döring, Nature 354 (1991) 463;
(b) A.L. Barra, D. Gatteschi, L. Pardi, A. Müller, J. Döring, J. Am. Chem. Soc. 114 (1992) 8509;
(c) D. Procissi, A. Lascialfari, E. Micotti, M. Bertassi, P. Carretta, Y. Furukawa, P. Kögerler, Phys. Rev. B 73 (2006) 184417;
(d) Y. Furukawa, Y. Nishisaka, K.I. Kumagai, P. Kögerler, F. Borsa, Phys. Rev. B 75 (2007) 220402;
(e) G. Chaboussant, R. Basler, A. Sieber, S.T. Ochsenbein, A. Desmedt, R.E. Lechner, M.T.F. Telling, P. Kögerler, A. Müller, H.U. Güdel, Europhys. Lett. 59 (2002) 291;
(f) S. Bertaina, S. Gambarelli, T. Mitra, B. Tsukerblat, A. Müller, B. Barbara, Nature 453 (2008) 203.

[5] M.B. Robin, P. Day, Adv. Inorg. Chem. Radiochem. 10 (1967) 247.

[6] (a) N. Suaud, A. Gaita-Ariño, J.M. Clemente-Juan, E. Coronado, Chem. Eur. J. 10 (2004) 4041;
(b) C.J. Calzado, J.M. Clemente-Juan, E. Coronado, A. Gaita-Ariño, N. Suaud, Inorg. Chem. 47 (2008) 5889.

[7] A. Müller, R. Sessoli, E. Krickemeyer, H. Bögge, J. Meyer, D. Gatteschi, L. Pardi, J. Westphal, K. Hovemeier, R. Rohlfing, J. Döring, F. Hellweg, C. Beugholt, M. Schmidtmann, Inorg. Chem. 36 (1997) 5239.

[8] (a) A. Barbour, R.D. Luttrell, J. Choi, J.L. Musfeldt, D. Zipse, N.S. Dalal, D.W. Boukhvalov, V.V. Dobrovitski, M.I. Katsnelson, A.I. Lichtenstein, B.N. Harmon, P. Kögerler, Phys. Rev. B 74 (2006) 014411;
(b) D. Gatteschi, B. Tsukerblat, A.L. Barra, L.C. Brunel, A. Müller, J. Döring, Inorg. Chem. 32 (1993) 2114.

[9] J.J. Borrás-Almenar, J.M. Clemente-Juan, E. Coronado, A.V. Palii, B. Tsukerblat, in: J.S. Miller, M. Drillon (Eds.), Double exchange. Magnetism: Molecules to Materials, Wiley-VCH, Weinheim, 2001, p. 155.

[10] D. Gatteschi, R. Sessoli, W. Plass, A. Müller, E. Krickemeyer, J. Meyer, D. Sölter, P. Adler, Inorg. Chem. 35 (1996) 1926.

[11] (a) J.M. Clemente-Juan, E. Coronado, A. Gaita-Ariño, C. Giménez-Saiz, G. Chaboussant, H.U. Güdel, R. Burriel, H. Mutka, Chem. Eur. J. 8 (2002) 5701;
(b) J.M. Clemente-Juan, E. Coronado, A. Gaita-Ariño, C. Giménez-Saiz, H.U. Güdel, A. Sieber, R. Bircher, H. Mutka, Inorg. Chem. 44 (2005) 3389.

[12] (a) K.Y. Choi, Y.H. Matsuda, H. Nojiri, U. Kortz, F. Hussain, A.C. Stowe, C. Ramsey, N.S. Dalal, Phys. Rev. Lett. 96 (2006) 107202;
(b) K.Y. Choi, N.S. Dalal, A.P. Reyes, P.L. Kuhns, Y.H. Matsuda, H. Nojiri, S.S. Mal, U. Kortz, Phys. Rev. B 77 (2008) 024406.

[13] (a) Y.V. Rakitin, Y.V. Yablokov, V.V. Zelentsov, J. Magn. Reson. 43 (1981) 288;
(b) J. Yoon, E.I. Solomon, Coord. Chem. Rev. 251 (2007) 379;
(c) X.M. Liu, M.P. de Miranda, E.J.L. McInnes, C.A. Kilner, M.A. Halcrow, Dalton Trans. (2004) 59;

(d) N. Kirchner, J. van Slageren, B. Tsukerblat, O. Waldmann, M. Dressel, Phys. Rev. B 78 (2008) 094426;
(e) W. Wernsdorfer, T.C. Stamatatos, G. Christou, Phys. Rev. Lett. 101 (2008) 237204.
[14] J.M. Clemente-Juan, H. Andres, J.J. Borrás-Almenar, E. Coronado, H.U. Güdel, M. Aebersold, G. Kearly, H. Büttner, M. Zolliker, J. Am. Chem. Soc. 121 (1999) 10021.
[15] (a) A. Müller, M. Luban, C. Schröder, R. Modler, P. Kögerler, M. Axenovich, J. Schnack, P. Canfield, S. Bud'ko, N. Harrison, Chemphyschem 2 (2001) 517;
(b) O. Waldmann, Phys. Rev. B 75 (2007) 012415;
(c) V.O. Garlea, S.E. Nagler, J.L. Zarestky, C. Stassis, D. Vaknin, P. Kögerler, D.F. McMorrow, C. Niedermayer, D.A. Tennant, B. Lake, Y. Qiu, M. Exler, J. Schnack, M. Luban, Phys. Rev. B 73 (2006) 024414;
(d) C. Schröder, H. Nojiri, J. Schnack, P. Hage, M. Luban, P. Kögerler, Phys. Rev. Lett. 94 (2005) 017205;
(e) I. Rousochatzakis, A.M. Läuchli, F. Mila, Phys. Rev. B 77 (2008) 094420.
[16] S.K. Pati, C.N.R. Rao, Chem. Commun. (2008) 4683.
[17] A. Müller, E. Beckmann, H. Bögge, M. Schmidtmann, A. Dress, Angew. Chem. Int. Ed. 41 (2002) 1162.
[18] (a) A. Müller, S.K. Das, S. Talismanov, S. Roy, E. Beckmann, H. Bögge, M. Schmidtmann, A. Merca, A. Berkle, L. Allouche, Y.S. Zhou, L.J. Zhang, Angew. Chem. Int. Ed. 42 (2003) 5039;
(b) A. Merca, E.T.K. Haupt, T. Mitra, H. Bögge, D. Rehder, A. Müller, Chem. Eur. J. 13 (2007) 7650;
(c) A. Merca, H. Bögge, M. Schmidtmann, Y. Zhou, E.T.K. Haupt, M.K. Sarker, C.L. Hill, A. Müller, Chem. Commun. (2008) 948.
[19] (a) A. Müller, Y.S. Zhou, L.J. Zhang, H. Bögge, M. Schmidtmann, M. Dressel, J. van Slageren, Chem. Commun. (2004) 2038;
(b) A. Müller, J. van Slageren, Y. Zhou, A. Merca, H. Bögge, M. Schmidtmann, M. Dressel (unpublished results).
[20] A. Müller, S. Sarkar, S.Q.N. Shah, H. Bögge, M. Schmidtmann, S. Sarkar, P. Kögerler, B. Hauptfleisch, A.X. Trautwein, V. Schünemann, Angew. Chem. 111 (1999) 3435.
[21] A. Müller, A.M. Todea, H. Bögge, J. van Slageren, M. Dressel, A. Stammler, M. Rusu, Chem. Commun. (2006) 3066.
[22] A.M. Todea, A. Merca, H. Bögge, J. van Slageren, M. Dressel, L. Engelhardt, M. Luban, T. Glaser, M. Henry, A. Müller, Angew. Chem. Int. Ed. 46 (2007) 6106.
[23] J. Schnack, M. Luban, R. Modler, Europhys. Lett. 56 (2001) 863.
[24] A. Müller, A.M. Todea, J. van Slageren, M. Dressel, H. Bögge, M. Schmidtmann, M. Luban, L. Engelhardt, M. Rusu, Angew. Chem. Int. Ed. 44 (2005) 3857.
[25] R. Schmidt, J. Richter, J. Schnack, J. Magn. Magn. Mater. 295 (2005) 164.
[26] J. van Slageren, O. Pieper, B. Lake, T. Guidi, H. Mutka, A.M. Todea, A. Müller, unpublished results (2007).
[27] A. Müller, H. Bögge, F.L. Sousa, M. Schmidtmann, D.G. Kurth, D. Volkmer, J. van Slageren, M. Dressel, M.L. Kistler, T.B. Liu, Small 3 (2007) 986.
[28] A. Müller, C. Beugholt, P. Kögerler, H. Bögge, S. Bud'ko, M. Luban, Inorg. Chem. 39 (2000) 5176.
[29] (a) R. Koch, O. Waldmann, P. Müller, U. Reimann, R.W. Saalfrank, Phys. Rev. B 67 (2003) 094407;
(b) H. Andres, R. Basler, A.J. Blake, C. Cadiou, G. Chaboussant, C.M. Grant, H.U. Güdel, M. Murrie, S. Parsons, C. Paulsen, F. Semadini, V. Villar, W. Wernsdorfer, R.E.P. Winpenny, Chem. Eur. J. 8 (2002) 4867;
(c) E.C. Yang, W. Wernsdorfer, S. Hill, R.S. Edwards, M. Nakano, S. Maccagnano, L.N. Zakharov, A.L. Rheingold, G. Christou, D.N. Hendrickson, Polyhedron 22 (2003) 1727;
(d) M. Moragues-Cánovas, M. Helliwell, L. Ricard, E. Rivière, W. Wernsdorfer, E. Brechin, T. Mallah, Eur. J. Inorg. Chem. (2004) 2219;
(e) A. Sieber, C. Boskovic, R. Bircher, O. Waldmann, S.T. Ochsenbein, G. Chaboussant, H.U. Güdel, N. Kirchner, J. van Slageren, W. Wernsdorfer, A. Neels, H. Stoeckli-Evans, S. Janssen, F. Juranyi, H. Mutka, Inorg. Chem. 44 (2005) 4315;
(f) C. Cao, S. Hill, H.P. Cheng, Phys. Rev. Lett. 100 (2008) 167206;
(g) J.M. Clemente-Juan, E. Coronado, J.R. Galán-Mascarós, C.J. Gómez-García, Inorg. Chem. 38 (1999) 55.
[30] J. Schnack, M. Brüger, M. Luban, P. Kögerler, E. Morosan, R. Fuchs, R. Modler, H. Nojiri, R.C. Rai, J. Cao, J.L. Musfeldt, X. Wei, Phys. Rev. B 73 (2006) 094401.
[31] C. Kittel, Phys. Rev. 120 (1960) 335.
[32] V.V. Kostyuchenko, Phys. Rev. B 76 (2007) 212404.
[33] (a) M. Brüger, J. Schnack (unpublished) (2008).;
(b) M. Brüger, PhD Thesis, University of Osnabrück, 2008.;
(c) T. Glaser, M. Heidemeier, E. Krickemeyer, H. Bögge, A. Stammler, R. Fröhlich, E. Bill, J. Schnack, Inorg. Chem. 48 (2009) 607.
[34] (a) R.A. Klemm, D.V. Efremov, Phys. Rev. B 77 (2008) 184410;
(b) Z.B. Li, K.L. Yao, Z.L. Liu, J. Magn. Magn. Mater. 320 (2008) 1759.
[35] R. Contant, A. Tézé, Inorg. Chem. 24 (1985) 4610.
[36] M. Zimmermann, N. Belai, R.J. Butcher, M.T. Pope, E.V. Chubarova, M.H. Dickman, U. Kortz, Inorg. Chem. 46 (2007) 1737.
[37] (a) S.S. Mal, U. Kortz, Angew. Chem. Int. Ed. 44 (2005) 3777;
(b) D. Jabbour, B. Keita, L. Nadjo, U. Kortz, S.S. Mal, Electrochem. Commun. 7 (2005) 841;
(c) M.S. Alam, V. Dremov, P. Müller, A.V. Postnikov, S.S. Mal, F. Hussain, U. Kortz, Inorg. Chem. 45 (2006) 2866;
(d) G. Liu, T.B. Liu, S.S. Mal, U. Kortz, J. Am. Chem. Soc. 128 (2006) 10103;
(e) G. Liu, T.B. Liu, S.S. Mal, U. Kortz, J. Am. Chem. Soc. 129 (2007) 2408.
[38] C. Pichon, P. Mialane, A. Dolbecq, J. Marrot, E. Rivière, B. Keita, L. Nadjo, F. Secheresse, Inorg. Chem. 46 (2007) 5292.
[39] A. Müller, M.T. Pope, A.M. Todea, H. Bögge, J. van Slageren, M. Dressel, P. Gouzerh, R. Thouvenot, B. Tsukerblat, A. Bell, Angew. Chem. Int. Ed. 46 (2007) 4477.
[40] S.S. Mal, N.H. Nsouli, M.H. Dickman, U. Kortz, Dalton Trans. (2007) 2627.
[41] S.S. Mal, M.H. Dickman, U. Kortz, A.M. Todea, A. Merca, H. Bögge, T. Glaser, A. Müller, S. Nellutla, N. Kaur, J. van Tol, N.S. Dalal, B. Keita, L. Nadjo, Chem. Eur. J. 14 (2008) 1186.
[42] (a) S.M. Gorun, S.J. Lippard, Inorg. Chem. 30 (1991) 1625;
(b) C. Cañada-Vilalta, T.A. O'Brien, E.K. Brechin, M. Pink, E.R. Davidson, G. Christou, Inorg. Chem. 43 (2004) 5505;
(c) J.K. McCusker, C.A. Christmas, P.M. Hagen, R.K. Chadha, D.F. Harvey, D.N. Hendrickson, J. Am. Chem. Soc. 113 (1991) 6114;
(d) C. Delfs, D. Gatteschi, L. Pardi, R. Sessoli, K. Wieghardt, D. Hanke, Inorg. Chem. 32 (1993) 3099;
(e) A. Ozarowski, B.R. McGarvey, J.E. Drake, Inorg. Chem. 34 (1995) 5558.
[43] (a) R.L. Carlin, Magnetochemistry, Springer Verlag, Berlin, 1986;
(b) O. Kahn, Molecular Magnetism, VCH, New York, 1993.
[44] (a) U. Kortz, N.K. Al-Kassem, M.G. Savelieff, N.A. Al Kadi, M. Sadakane, Inorg. Chem. 40 (2001) 4742;
(b) A.C. Stowe, S. Nellutla, N.S. Dalal, U. Kortz, Eur. J. Inorg. Chem. (2004) 3792;
(c) U. Kortz, S. Nellutla, A.C. Stowe, N.S. Dalal, J. van Tol, B.S. Bassil, Inorg. Chem. 43 (2004) 144.
[45] B. Cage, F.A. Cotton, N.S. Dalal, E.A. Hillard, B. Rakvin, C.M. Ramsey, J. Am. Chem. Soc. 125 (2003) 5270.
[46] U. Kortz, S. Nellutla, A.C. Stowe, N.S. Dalal, U. Rauwald, W. Danquah, D. Ravot, Inorg. Chem. 43 (2004) 2308.
[47] (a) L.H. Bi, U. Kortz, Inorg. Chem. 43 (2004) 7961;
(b) S. Nellutla, J. van Tol, N.S. Dalal, L.H. Bi, U. Kortz, B. Keita, L. Nadjo, G.A. Khitrov, A.G. Marshall, Inorg. Chem. 44 (2005) 9795.
[48] N. Laronze, J. Marrot, G. Hervé, Chem. Commun. (2003) 2360.
[49] I.D. Brown, D. Altermatt, Acta Cryst. B 41 (1985) 244.
[50] (a) V.H. Crawford, H.W. Richardson, J.R. Wasson, D.J. Hodgson, W.E. Hatfield, Inorg. Chem. 15 (1976) 2107;
(b) E.A. Buvaylo, V.N. Kokozay, O.Y. Vassilyeva, B.W. Skelton, J. Jezierska, L.C. Brunel, A. Ozarowski, Inorg. Chem. 44 (2005) 206.
[51] (a) E. Gojon, J. Gaillard, J.-M. Latour, J. Laugier, Inorg. Chem. 26 (1987) 2046;
(b) S. Meenakumari, M. Lakshiminarayanan, S.K. Tiwary, A.R. Chakravarty, Inorg. Chem. 34 (1995) 5091;
(c) A.A. Doyle, S. Parsons, G.A. Solan, R.E.P. Winpenny, J. Chem. Soc., Dalton Trans. (1997) 2131;
(d) Y. Song, J.C. Liu, Y.J. Liu, D.R. Zhu, J.Z. Zhuang, X.Z. You, Inorg. Chim. Acta 305 (2000) 135;
(e) G.S. Papaefstathiou, C.P. Raptopoulou, A. Tsohos, A. Terzis, E.G. Bakalbassis, S.P. Perlepes, Inorg. Chem. 39 (2000) 4658.
[52] (a) M. Bösing, A. Noh, I. Loose, B. Krebs, J. Am. Chem. Soc. 120 (1998) 7252;
(b) B. Botar, T. Yamase, E. Ishikawa, Inorg. Chem. Commun. 4 (2001) 551;
(c) T. Yamase, B. Botar, E. Ishikawa, K. Fukaya, Chem. Lett. (2001) 56;
(d) P. Mialane, J. Marrot, E. Riviere, J. Nebout, G. Hervé, Inorg. Chem. 40 (2001) 44;
(e) D. Drewes, G. Vollmer, B. Krebs, Z. Anorg. Allg. Chem. 630 (2004) 2573.
[53] A. Merca, A. Müller, J. van Slageren, M. Läge, B. Krebs (unpublished 2008).
[54] N. Ishikawa, M. Sugita, W. Wernsdorfer, Angew. Chem. Int. Ed. 44 (2005) 2931.
[55] R.E.P. Winpenny, Angew. Chem. Int. Ed. 47 (2008) 7992, with graphical abstract on page 7971 (see also C. Schlegel, J. van Slageren, M. Manoli, E. K. Brechin, M. Dressel, Phys. Rev. Lett. 101 (2008) 147203).